

## KINETIC AND THERMODYNAMIC STUDIES OF TRIVALENT ARSENIC REMOVAL BY INDIUM-DOPED ZINC OXIDE NANOPOWDER

L. KHEZAMI<sup>a</sup>, KAMAL K. TAHA<sup>a,b\*</sup>, A. MODWI<sup>a,c</sup>

<sup>a</sup>*Department of Chemistry, College of Sciences, Al-Imam Muhammad Ibn Saud University(IMSU), ,Riyadh 11623, Saudi Arabia.*

<sup>b</sup>*Dept. Chem.and Ind. Chem., College of Applied & Industrial Sci., University of Bahri, Sudan*

<sup>c</sup>*Department of Chemistry, College of Science, Omdurman Islamic University, Omdurman, Sudan*

The uptake of trivalent arsenic from aqueous solutions onto indium-doped ZnO (IZO) nanopowder was studied. The nanopowder was fabricated using a modified sol-gel method under supercritical drying conditions of ethanol. X-ray diffraction and nitrogen adsorption techniques were employed to characterize the IZO nanopowder. The N<sub>2</sub> adsorption isotherms reveal that pure and doped ZnO nanopowders were mesoporous materials. Removal of arsenite ions from the solutions by IZO nanopowder was conducted in a batch-mode reactor. The impact of initial concentration, indium-doping dose, temperature and pH were considered. Arsenite removal was pH sensitive scoring its maximum elimination capacity at pH 3 and 7. The adsorption equilibrium was well delineated by Langmuir isotherm. Data were further found to comply with the pseudo-second-order kinetic law, and the process was spontaneous endothermic physisorption.

(Received October 16, 2016; Accepted December 28, 2016)

*Keywords:* Nanostructures; IZO; trivalent arsenic; Adsorption; kinetics.

### 1. Introduction

Heavy metals ions are disposed into the environment due to human anthropogenic activities. As they are toxic, they are hazardous to living organisms and environment, especially when tolerance levels are exceeded. Arsenic is a lethal pollutant that results from industrial and other anthropogenic activities as well as its natural abundance in ground water. Wastewater effluents from the pharmaceutical, pesticidal, chemical, metallurgical, mining, and leather tanning industries have significant contribution to arsenic pollution. Arsenic is present in the trivalent As(III) and pentavalent As(V) form termed as arsenites and arsenates, respectively, with the former considered highly perilous than the latter. Sicknesses such as dermal, lungs and bladder cancer, as well as gastroenteritis [1 - 4] were related to the contact with arsenic. The permissible limit for arsenic in industrial wastewaters in most developed countries such as Japan is about 10  $\mu\text{g L}^{-1}$ [5].

Methods of heavy metals ions elimination like precipitation, filtration and ion exchange are commonly employed. Such techniques are less adopted as they are expensive, unsuitable to daily life activities. Adsorption is alternative versatile technique extensively applied for water systems purification from pollutants. Alumina, silica, metal hydroxides [6, 7] activated carbon [8, 9], and zeolites [8], or natural products such as clays [10] and red soil [11] were utilized for toxic metal ions elimination. In previous studies, IZO nanopowder has been used as an adsorbent for heavy metals [12 – 14].

This study aimed to assess the adsorption efficiency of IZO nanopowder for As(III) ion selimination from aqueous solutions. The effects of indium-doping percentage, pH and initial As(III) concentration were evaluated through batch adsorption experiments. First- and second-

---

\*Corresponding author: kamalth60@gmail.com

order rate representations were used to delineate the adsorption kinetics at different initial arsenite concentrations, pH 3 and 7 at 25 °C. In addition, adsorption capacities of As(III) on IZO adsorbent were correlated by Langmuir, Freundlich, and Dubinin–Radushkevich (D-R) isotherms at the two different pH values. Constants derived from the adsorption thermodynamic studies were evaluated.

## 2. Experimental

### 2.1. IZO nanopowder synthesis

IZO nanopowder was synthesized by the sol–gel procedure following EL MIR *et al.* [16, 17]. IZO nanopowder were produced by mixing zinc acetate dehydrate and a sufficient volume of methyl alcohol. The mixture was magnetically stirred for 10 minutes, then indium chloride equivalent to different ratio of  $[In]/([Zn]+[In])$  was added to the mixture. After extra stirring for 15 minutes, the mixture was placed in an autoclave and dried under supercritical conditions of ethanol.

### 2.2. IZO Characterization

The crystallite pattern of the obtained IZO nanopowders at different doping concentrations was identified using X-ray diffraction (XRD). While its porosity, was characterized by nitrogen adsorption using ASAP 2020 Micromeritics analyzer. Prior to each analysis, ZnO and ZnO: Inx% samples were out gassed at 250 °C for 6 h in vacuum. The nanopowder's surface area and pore size and diameter were calculated from the BET equation and Lippens and de Boer [18] t-plot method.

### 2.3. Solutions Preparation:

An stock solution of 1000 mg L<sup>-1</sup> was prepared from a commercial pure As[III] standard. Solutions required to carry out the experiments were prepared by diluting the stock solution to intended concentrations. The solutions pH was fixed using HNO<sub>3</sub> and NaOH. All reagents used were of high purity and were used as received.

### 2.4. Batch-mode adsorption

Batch mode experiments were performed by mixing 13 mg of IZO and 25 ml of a known As(III) molarity and pH in 50 ml Erlenmeyer flask. Adsorption studies were conducted at different pH values (2.3–9.5) and initial As(III) concentration (5–30 mg L<sup>-1</sup>) to obtain equilibrium isotherms. Several flasks were placed on a magnetic stirrer and stirred at 550 rpm. About 15 ml of suspension was sampled from each flask after 12 h, centrifuged with Hettich Zentrifugen EBA 20), and then passed through 0.25 µm cellulose acetate filter. The As(III) content in filtrate was estimated using atomic emission spectroscopy (Genius, ICP-EOS, Germany). All experiments were carried in triplicate and their mean was used.

The mass of metal ions adsorbed ( $q_e$ ) per gram of IZO (mg g<sup>-1</sup>), and the percentage of removal values were obtained using the relationships:

$$q_e = \frac{(C_0 - C_e) * V}{m} \quad (1)$$

$$\% \text{Removal} = \frac{(C_0 - C_e)}{C_0} * 100 \quad (2)$$

Here  $C_0$  and  $C_e$  are the As(III) ion concentrations (mg L<sup>-1</sup>) at  $t = 0$  and equilibrium respectively, whereas  $V$  (L) and  $m$ (g) are the solution volume and dry adsorbent weight.

### 3. Results and Discussion

#### 3.1. IZO nanopowder characterization

##### 3.1.1. XRD

Fig. 1 portrays the XRD structures of IZO recorded in  $2\theta$  degree. The obtained peaks were identical to the hexagonal wurtzite structure ZnO. For all indium-doping percentages, no peak corresponding to indium or indium oxide phases were observed, which denoted that In ions have perforated into the lattices of ZnO. Thus there is no peak corresponding to a secondary phase of indium. At the highest In doping ratio (5 %), the peak 101 has been enhanced indicating a preferential growth orientation in the (101) plane [19]. A similar behavior has been observed for aluminum doped ZnO[20]. Nanoparticle size was estimated using XRD data and applying Scherer equation:

$$G = \frac{0.9\lambda}{\beta \cos\theta_{\beta}} \quad (3)$$

here  $\lambda$  is the X-ray wavelength ( $\lambda = 1.78901 \text{ \AA}$  for Co  $K_{\alpha}$ ),  $\beta$  the full width at half maximum (FWHM) of the diffraction peak  $\theta_{\beta}$  (in rad). The mean grain size of nanoparticles was almost equal to 53 nm. The values of crystallite size obtained in this work is comparable with the 65 nm of undoped ZnO and 58 nm doped sample reported by Hjiri *et al.* [21] and Ben Ayadi *et al.*[22].

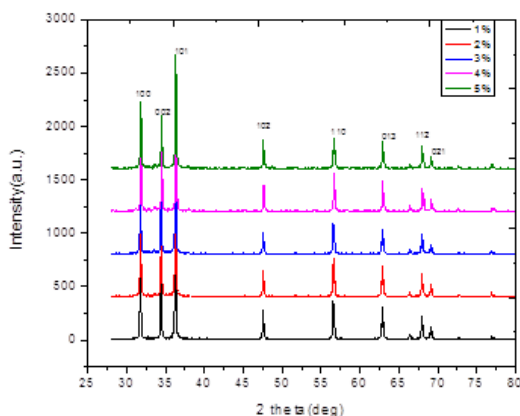


Fig. 1 XRD patterns of indium doped ZnO powder with different indium concentrations

##### 3.1.2. Nitrogen adsorption

Isotherm shape provides information on pore size, which is usually categorized as micropore, mesopore or macropore. For instance, Fig.2 depicts the evolution of  $N_2$  adsorption–desorption isotherms for pure ZnO and IZO nanopowders. These isotherms were obviously type II, with a hysteresis of H4 type, according to the IUPAC or Brunauer’s categorization of sorption isotherms [23]. At elevated relative pressure  $P/P_0$ , the hysteresis of H4 type was due to the filling up of meso pores by capillary condensation, indicating a shape of pores that was flatter instead of cylindrical. Particle size, pore characteristics, and BET surface area are recorded in Table 1. BET surface area was found to increase with increased indium-doping concentration.

Table 1 Main characteristics of IZO nanopowders

Nanoparticles	Grain Size (nm)	Pore diameter (nm)	Pore volume (cm <sup>3</sup> g <sup>-1</sup> )x10 <sup>2</sup>	Surface BET (m <sup>2</sup> g <sup>-1</sup> )
ZnO	62.00	46.5	7.1	8.25
ZnO:In 1%	61.00	14.3	5.0	8.18
ZnO:In 2%	60.71	18.4	9.5	13.57
ZnO:In 3%	61.70	24.2	14.5	20.07
ZnO:In4%	62.62	12.2	6.3	17.92
ZnO:In 5%	63.11	18.3	11.5	19.51

The surface area significantly increased from 8 to 20 m<sup>2</sup> g<sup>-1</sup> with increased doping ratio from 1% to 3%, and then slightly decreased for nanopowders of 4% and 5% doping ratio. Results showed increased mean diameter of pores (from 14.3 to 24.1 nm) and total volume ( $5 \times 10^{-2}$  to  $14 \times 10^{-2}$  cm<sup>3</sup>g<sup>-1</sup>) for samples with doping ratio ranging from 1% to 3%, followed by a gradual decrease for samples with 4% and 5% doping doses. This finding was in agreement with XRD results (Table 1 and Fig. 1).

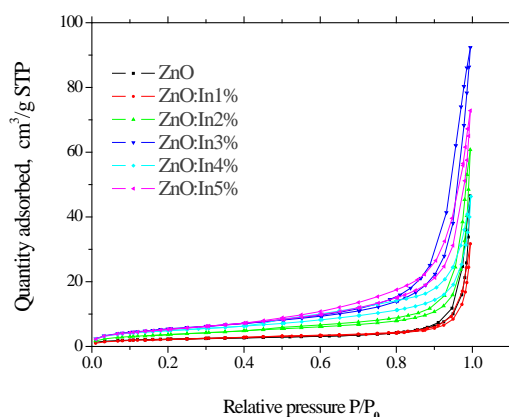


Fig.2 Adsorption-desorption isotherms of N<sub>2</sub> at 77 K of pure and Indium doped zinc oxide nanopowders

Al Dahoudi *et al.*[24] have reported a very similar trend of BET surface area for crystalline IZO nanopowder synthesized by hydrothermal treatment. They observed that the incorporation of indium ions into ZnO particles obviously affected both the growth of ZnO lattice and nanostructure. They further demonstrated an evolution of nanoparticle shape, i.e., rod-like pure ZnO progressively transformed to spherical, thereby leading to decreased nanoparticle size with increased indium-doping concentration.

The BET surface area was reported to enlarge from 6.4 to 20 m<sup>2</sup>g<sup>-1</sup> when ZnO was doped with Al [25]. Identical findings were reported by Wang *et al.*[26] who found that the BET surface area of boron doped titanium oxide increased when the ratio was increased from 0.11 to 0.57 (17 to 34 m<sup>2</sup>g<sup>-1</sup>). Whereas, when the ratio was raised to 1.14 the surface area dropped drastically to 13 m<sup>2</sup>g<sup>-1</sup>.

### 3.2. Arsenic adsorption

#### 3.2.1. Effect of indium-doping concentration on arsenic removal

In this study, 10 mg of IZO adsorbent with different indium-doping concentrations (1% to 5%) were added to 25 ml of 15 mg L<sup>-1</sup> metal ion solution. Fig.3 illustrates the impact of indium-doping percentage on the adsorption of As(III) ions by IZO.

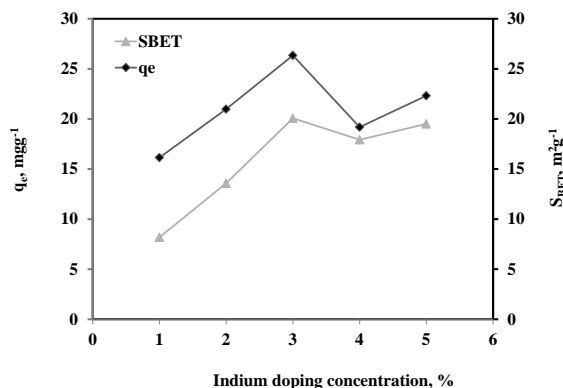


Fig.3 Influence of Indium doping concentration on the amount of adsorption and specific surface area

The amount of adsorbed metal ions  $q_e$  sharply increased with increased doping dose, reaching a maximum of  $26.34 \text{ mgg}^{-1}$  at 3% doping dose. Afterwards, this optimum  $q_e$  declined with increased doping dose. The maximum amount of adsorption was obtained at 3% doping dose, indicating that the powder was highly electrical conducting and that adsorption may be controlled by Van der Waals forces. Fig. 3 also shows a perfect coherence between the values of surface area of IZO nanopowder and its capacity of adsorption at various indium-doping doses. Thus, adsorption capacity may be enhanced by BET surface area increase, similar to the report of Bhattacharya *et al.* [5]. They showed that As(III) adsorption on different uncalcined and calcined aluminum hydroxide powders mostly depended on surface area. During the removal of arsenic by Mn-doped iron oxide Garcia *et al.* [27], observed an enhancement in its binding when the Mn ratio was 50 % and a decrease as the ratio was increased to 75 %. They attributed the first case to the substitution of Mn in the oxide lattice, while at higher ratio a second phase of Mn was formed leading to the suppression of arsenic binding.

### 3.2.2. Effect of the pH on arsenic removal

Working solution pH is considered one of the key factors controlling heavy-metal removal [28]. At pH 0–9, As(III) is stable neutral  $\text{H}_3\text{AsO}_3$ , whereas  $\text{H}_2\text{AsO}^{-3}$ ,  $\text{HAsO}_2^{-3}$ , and  $\text{AsO}_3^{-3}$  exist as stable entity at pH 10–12, 13, and 14, respectively. Numerous investigations conducted within this range have indicated maximum arsenic ion removal using different adsorbents [10 -15, 17]. Thus, the pH influence on As(III) adsorption was investigated within pH 2.3–9.5 at  $25^\circ\text{C}$ , with the initial As(III) concentration fixed at  $20 \text{ mgL}^{-1}$  and 10 mg of IZO nanoparticles. The results of the pH effect on adsorption performance are illustrated in Fig.4. The removal of As(III) increased with increased initial solution pH, reached the first maximum at pH 3.0 ( $48.8 \text{ mgg}^{-1}$ ), and then declined at pH 6.0. The maximum of adsorption quantity increased with increased pH to reach again a second maximum ( $40.7 \text{ mgg}^{-1}$ ), followed by a drastic decrease at pH 9.5.

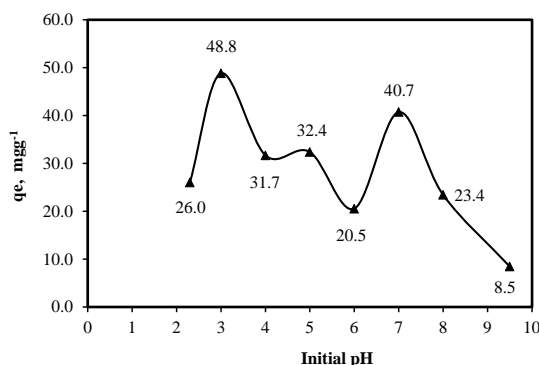


Fig.4 The effect of pH on the adsorption of As (III) onto indium doped ZnO at  $25^\circ\text{C}$ .

Indeed, arsenite ions removal by IZO is highly pH dependent, as has been reported by several investigators [6–11], who showed enhanced As(III) adsorption by various adsorbents at pH 0–9. Kelly and Tarek [8] showed that the adsorption of arsenates and arsenites on iron-treated activated carbon and zeolites was greater at pH 7.0–11.0. Yunhai *et al.* [9] studied the removal of chromium and arsenic by activated carbon and found that As(III) adsorption reached the upper limit at pH 7.0. Pravin *et al.* [11] announced that the removal As(III) by red soil was independent of pH within the range of 4–10, with increased adsorption at the acidic pH range. Upon investigating the adsorption of As(III) on Jang *et al.* [29] showed that the optimum binding of the arsenic ions to iron oxide nanomaterials was at pH 6 to 9 and a sharp decrease was at pH 10. Thi *et al.* [30] reported an optimum adsorption of As(III) on iron magnetic particles at pH 7.0 and less at pH < 5 due to instability of the adsorbent at low pH values. An utmost adsorption was achieved at pH 3 by Garcia *et al.* [27] for As(III) onto mixed ferrite and hausmannite nanomaterials. An increase in arsenic removal in a pH range of 2.8–3.8 was attributed to an increase of de protonated arsenic species [31].

### 3.2.3 Kinetic study

The pseudo-first- and pseudo-second-order kinetic representations were employed to speculate the adsorption data of As(III) relation to time. The first-order law is illustrated by the equation [32]:

$$\ln(q_e - q_t) = \ln(q_e) - k_1 \cdot t \quad (4)$$

Here  $q_e$  and  $q_t$  ( $\text{mgg}^{-1}$ ) are the masses of As(III) adsorbed by a gram of IZO at equilibrium and time  $t$  (min), respectively, and  $k_1$  ( $\text{min}^{-1}$ ) is the rate constant. The intercept and slope of the  $\ln(q_e - q_t)$  against  $t$  will give  $q_e$  and  $k_1$  values respectively. The second rate law is given by the formula [33]:

$$\frac{t}{q_t} = \frac{1}{k_2 \cdot q_e^2} + \frac{t}{q_e} \quad (5)$$

$k_2$  stands for rate constant ( $\text{g}(\text{mgmin})^{-1}$ ) value. The constants  $q_e$  and  $k_2$  are obtained from  $t/q_t$  against  $t$ . Alternatively,  $k_2$  is computed using  $t_{1/2}$  (half-adsorption time) expressed in equation (6). The time for half of the maximal mass of metal ion adsorbed is indicated as  $t_{1/2}$ .

$$t_{1/2} = \frac{1}{k_2 q_e} \quad (6)$$

Values of  $t_{1/2}$ , as well as two models variables, are reported in Table 2.

Table 2 The adsorption kinetics parameters at different concentrations and pH

pH	Initial conc. ( $\text{mgL}^{-1}$ )	$t_{1/2}$ (min)	$q_{e(\text{exp})}^a$ ( $\text{mgg}^{-1}$ )	First-order			Second-order		
				$k_1 \times 10^2$ ( $\text{min}^{-1}$ )	$q_{e(\text{cal})}^b$ ( $\text{mgg}^{-1}$ )	$r^2$	$k_2 \times 10^4$ ( $\text{gmg}^{-1}\text{min}^{-1}$ )	$q_{e(\text{cal})}^b$ ( $\text{mgg}^{-1}$ )	$r^2$
3	10	84.28	50	1.54	42.77	0.958	2.46	48.31	0.987
	20	71.92	81	1.04	64.72	0.9991	1.68	82.64	0.9967
	30	50.95	117	0.85	91.30	0.9553	1.6	119.05	0.9954
7	10	129.92	43	0.45	38.70	0.9782	1.85	41.67	0.9951
	20	96.77	74	0.56	65.01	0.9742	1.41	73.53	0.9913
	30	80.75	99.05	0.64	77.39	0.9553	1.20	101.01	0.9933

<sup>a</sup>: experimental data

<sup>b</sup>: calculated data from models

The sorption data time relation for As(III) on IZO is displayed in Figure 5 for three initial concentrations and the optimum pH of 3 and 7 for all experiments. In all experiments, results showed starting speedy rise in adsorption capacity  $q_t$ , that becomes steady after about 180 minutes.

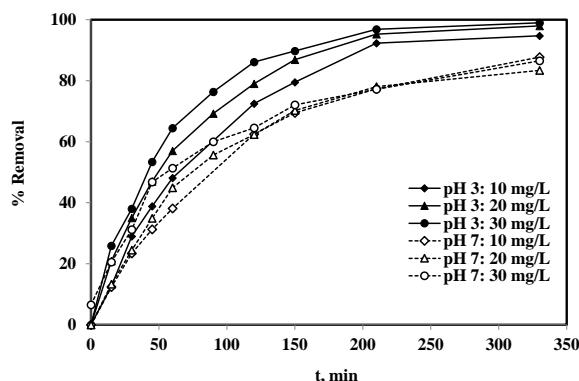


Fig.5 Effect of contact time on the adsorption of As(III) on IZO nanoparticles with different initial concentrations of As (III) ions pH 3.0 and 7.0 at 25 °C.

The relevance of kinetics data was negotiated by the value of the coefficient  $r^2$  tabulated in Table 2. Remarkably, the  $r^2$  values for the pseudo-first-order law is always  $<0.98$ , (Fig.6(a)), which indicates poor correlation. The data exhibits a significant difference between the theoretical  $q_e$  value and that obtained practically.

In contrast, using the pseudo-second-order representation resulted in better regression coefficients values i.e. all  $>0.99$  (Fig.6(b)). Moreover, the  $q_e$  value obtained experimentally matches that derived mathematically, as reported in Table 2; therefore, it can be concluded that the As(III) adsorption follows the second-order law. In literature, many studies have indicated similar finding [26, 34, 35].

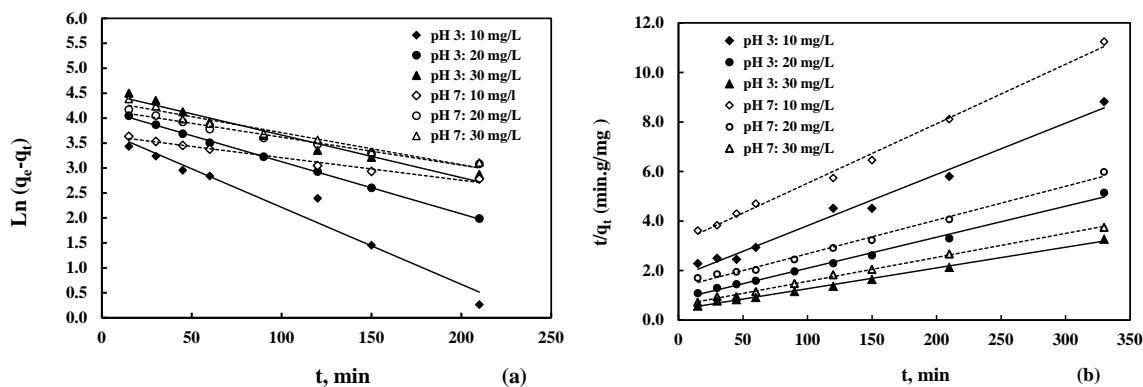


Fig.6 Pseudo-first order (a) and pseudo-second order (b) kinetic equation for adsorptions of As(III) on indium doped zinc oxide at different initial concentrations pH 3.0 and 7.0 at 25 °C.

### 3.2.4 Mechanism of adsorption

The adsorbed species may also be transported from the solution bulk to the solid phase by intra-particle diffusion/transport operation. The intra-particle diffusion is a controlling step of a number of adsorption processes. The likelihood of intra-particle diffusion is investigated by the Weber and Morris diffusion mode [36 -38]:

$$q_t = k_{dif} \cdot t^{1/2} + C \quad (7)$$

The values of  $C$  and the intra-particles speed constant  $k_{dif}$ , are respectively, derived from the slope and intercept of  $q_t$  against  $t^{1/2}$  graph. The value of the constant  $C$  stipulates the solution boundary layer thickness. The  $k_{dif}$  values for the arsenic ions adsorption at two pH values are computed and reported (Fig. 7 and Table 3). The uptake of As(III) at the surface of the adsorbent may be governed by the intra-particle diffusion kinetic formula, since,  $q_t$  and  $t^{1/2}$  hold a linear correlation.

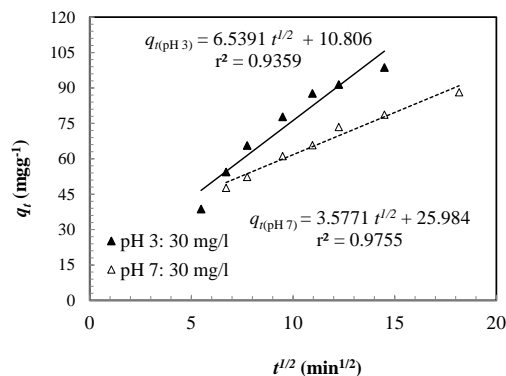


Fig. 7  $q_t$  versus  $t^{1/2}$  plot for the intraparticle diffusion

Besides, the regression coefficient values are more than 0.94 denoting the relevance of the data the model. The intra-particle diffusion diagrams are shown in Fig. 7, where the main parameters of this model are determined and gathered in Table 3. The thickness of boundary layer is strongly correlated to the intercept values. The larger intercept of the graph ( $C$  value, Table 3) signifies a greater boundary layer effect.

Table 3 The intraparticle diffusion model constants for the As(III) ions adsorption onto IZO.

pH	$k_{dif1}$ , mg/g.min <sup>1/2</sup>	$C$	$r^2$
3	6.5391	10.806	0.9359
7	3.5771	25.984	0.9755

As can be seen from Fig. 7, the graph is linear, with a graph not passing through the origin. This observation can be attributed to some level of boundary layer control. Such behavior is an indication that the intra-particle diffusion is not the sole rate controlling step, as other kinetic processes may influence the adsorption rate of adsorption. In other words, all of these operations are operating concurrently[39].

### 3.2.5 Equilibrium study

As(III) adsorption data were analogized with the Langmuir, Freundlich, and D-R models:

$$\frac{C_e}{q_e} = \frac{1}{Q_0} C_e + \frac{1}{Q_0 \cdot b} \quad \text{linear form of Langmuir equation} \quad (8)$$

$$\log q_e = \frac{1}{n} \log C_e + \log k \quad \text{linear form of Freundlich equation} \quad (9)$$

$$\log q_e = \log q_{max} - \beta \varepsilon^2 \quad \text{linear form of D-R equation} \quad (10)$$

The mass of As(III) adsorbed by one gram of IZO is  $q_e$  ( $\text{mg g}^{-1}$ ), the solute concentration  $C_e$  is expressed in ( $\text{mgL}^{-1}$ ),  $Q_0$  is the concentration of solid-phase required to form a monolayer on adsorption sites [28], and  $b$  is a coefficient associated with the free energy of adsorption ( $\Delta G_{ads}$ ). The terms  $k$  and  $n$  of Freundlich equation are connected with the strength and distribution of the adsorptive bond [32]. The coefficient  $\beta$  is related to ( $\Delta G$ ) of adsorption ( $\text{mol}^2\text{kJ}^{-1}$ ), and  $\varepsilon$  is the Polanyi potential ( $\text{kJmol}^{-1}$ ) expressed as:

$$\varepsilon = RT \log\left(1 + \frac{1}{C_e}\right) \quad (11)$$

Langmuir model suggests no dependence of ( $\Delta G_{ads}$ ) on surface coverage. This model also anticipates solid surface saturation ( $Q_0=q_e$ ) due to adsorbate monolayer coverage at large  $C_e$  values, while at small  $C_e$  linear adsorption takes place. The constants  $Q_0$  and  $b$  are derived from the slope and intercept of (Eq. 8) graph. The Langmuir representation is also indicated by a dimensionless separation coefficient  $R_L$  that delineates the category of isotherm:

$$R_L = \frac{1}{1 + b \cdot C_0} \quad (12)$$

where, the term  $C_0$  represents the solute concentration at  $t = 0$ . The value of  $R_L$  confirms the viability of adsorption. The process is irreversible, favorable, linear or unfavorable, when  $R_L$  values are  $= 0, < 1, = 1$  and  $> 1$  respectively.

The coefficients  $k$  and  $n$  can be derived from the slope and intercept of  $\log q_e$  against  $\log C_e$  graph respectively (Eq. 9). The term  $k$  represents the amount of solute adsorbed when  $C_e = 1$ , whereas, the  $1/n$  value quantifies sorption strength and surface heterogeneity [40]. When  $n = 1$ , the two phases separation concentration independent. The case of  $n > 1$  is the most ordinary and correlates with the L-type Langmuir model [41], while  $n < 1$  is indicative of collective sorption [42] bringing in a strong adsorbate molecules interactions. For the D-R model, the slope of the  $\log q_e$  versus  $\varepsilon^2$  (Eq. 10) gives the value of  $\beta$ . Knowledge of the value of this coefficient permits calculation of the mean value of activation energy of adsorption  $E$ , which is indicative of the physical or chemical nature of adsorption [43]. The value of  $E$  can be determined from the following equation [44]:

$$E = \frac{1}{\sqrt{2\beta}} \quad (13)$$

From the equilibrium study, isotherm data were obtained by testing the two optimum values of pH, i.e., 3 and 7, and then pH effect was determined at As(III) concentrations ranging from 5 to 55  $\text{mgL}^{-1}$ , 25 °C and 4 h contact time. The three isotherms are graphically plotted in Fig. 8 the two pH values. The equilibrium constants calculated by linearized Langmuir, Freundlich, and D-R equations are given in Table 4.

Table 4 Langmuir and Freundlich and Dubinin-Radushkevich models parameters,  $R_L$  and regression coefficients.

pH	Langmuir constants				Freundlich constants			Dubinin-Radushkevich constants			
	$q_e$ ( $\text{mg g}^{-1}$ )	$b$ ( $\text{L mg}^{-1}$ )	$r^2$	$R_L$	$n$	$K$	$r^2$	$q_{max}$ ( $\text{mg g}^{-1}$ )	$\beta$ ( $\text{mol}^2\text{kJ}^{-1}$ )	$E$ ( $\text{kJ mol}^{-1}$ )	$r^2$
3	104.17	0.3902	0.9931	0.0457	2.63	56.86	0.922	68.35	0.1628	1.75	0.9115
7	83.34	0.3221	0.9998	0.0454	2.51	25.57	0.9142	55.92	0.1927	1.61	0.9179

Finding out the model that gives the best fitting to the adsorption of As(III) on the nanoparticles powder is based on the value of the correlation coefficient ( $r^2$ ). Having a look at Table 3, the ( $r^2$ ) values for the Langmuir model is the highest ( $\approx 1.0$ ), denoting its best fit to adsorption data at both pH values. Similarly, Zeng [7] investigated the adsorption of arsenic on Fe(III)-Si binary oxide adsorbent and found a good matching of his data with the Langmuir isotherm. Meanwhile, Kelly and Tarek [8] showed that isotherm data of the adsorption of arsenite onto iron-treated activated carbon and zeolites were better fitted by the Freundlich equation. Table 3 indicates that the Langmuir, Freundlich, and D-R parameters  $Q_0$ ,  $k$ , and  $q_{max}$ , respectively, were higher at pH 3.0 than at pH 7.0. This finding confirmed that at this acidic pH, As(III) capacity adsorption was larger. Moreover, maximum adsorption capacities estimated from the Langmuir model were 104.17 and 83.34 mg of arsenite per gram of nanoparticles at pH 3 and 7, respectively. Table 3 also shows that the very low values of the separation factor,  $R_L$ , attested to the favorable sorption power of IZO nanopowder. At both pH values, the  $n$  values greater than 1 are indicative of a Langmuir process and of very weak interactions between molecules of solute [32]. However, the influence of the experimental conditions upon the parameter  $n$  is not obvious. According to the coefficient  $R_L$  values, the present adsorption systems revealed all favorable with IZO. Moreover, the very low values of free energy 1.75 and 1.61  $\text{kJ mol}^{-1}$ , estimated from D-R model, for pH 3 and 7 respectively, are indicative of a physisorption process [40 – 45].

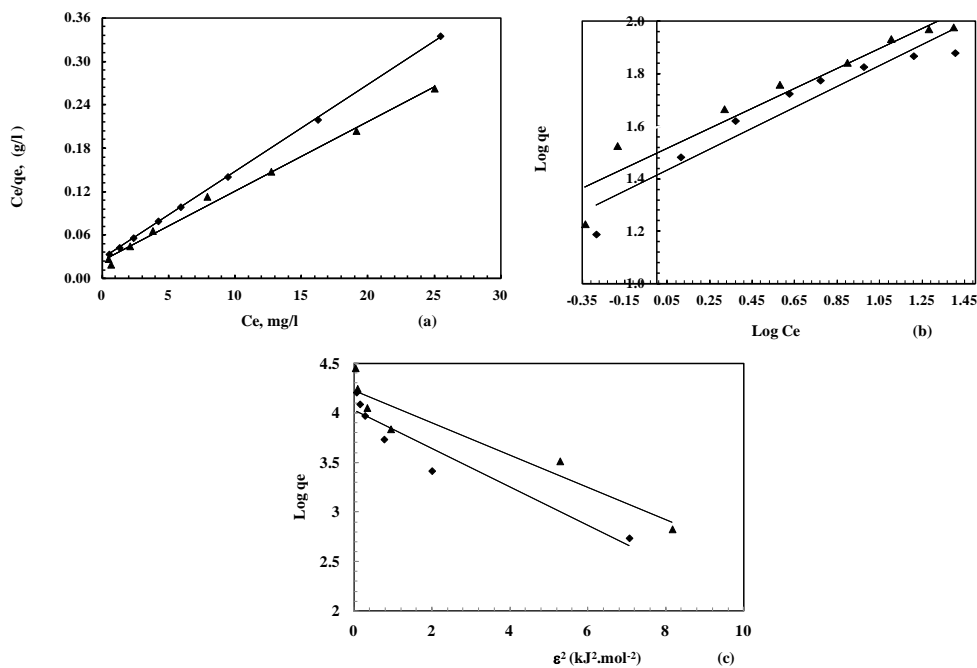


Fig 8 Langmuir (a) and Freundlich (b) D-R (c) linear isotherms at 25 °C for the adsorption of As(III) at : (♦) pH = 3.0 and (▲) pH = 7.0.

### 3.2.5 Effect of temperature in the adsorption process

Temperature is a detrimental factor in adsorption, therefore its effect was studied at 298, 313 and 328 K. The As(III) removal increases with the rise in temperature as displayed by the Langmuir graph (Fig. 9). The compliance of the adsorption data with Langmuir model for the chosen temperatures is evidenced by the correlation coefficient ( $r^2$ ) values shown in Table 5.

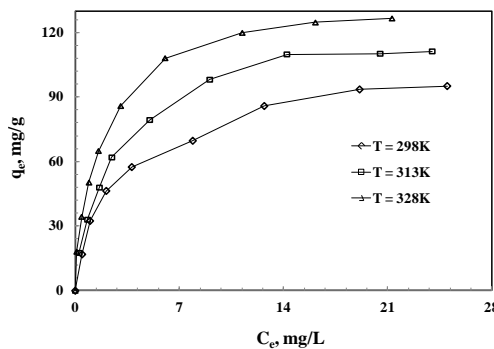


Fig. 9 Langmuir isotherms for adsorption of As (III) onto doped indium ZnO nanopowder at different temperatures

Table 5 Equilibrium constants for the removal of heavy metal ions at different temperatures.

T(K)	Langmuir constants				Freundlich constants		
	$q_m(\text{mgg}^{-1})$	$b(\text{Lmg}^{-1})$	$R_L$	$r^2$	$n$	$k_f$	$r^2$
298	104.2	0.390	0.9097	0.9931	2.630	56.8	0.9220
313	125.0	0.534	0.9241	0.9930	2.645	114.2	0.9260
328	142.9	0.875	0.9360	0.9920	2.670	118.4	0.9590

The Freundlich constant  $n$  value is more than 1.0 for the three chosen temperatures. The larger deviation of  $n$  from unity indicates greater distribution of surface bond energies of arsenic adsorption on indium doped zinc oxide nanopowder [41]. The values of the Freundlich constant  $n$  are greater than the unit. Therefore, nanoparticles ZnOIn 3% exhibits a wider As(III)-surface bond energies distribution as a result of temperature rise[41].

The thermodynamic functions: enthalpy change ( $\Delta H^0$ ), free energy change ( $\Delta G^0$ ) and entropy change ( $\Delta S^0$ ) for the adsorption of As(III) by the adsorbent are obtained using the relations:

$$\Delta G^0 = -R.T.\ln K_a \quad (14)$$

$$\Delta S^0 = \frac{\Delta H^0 - \Delta G^0}{T} \quad (15)$$

The  $K_a$  value is computed by the formula  $K_a = Q_0 \cdot b$ . The  $\Delta H^0$  value the slope of  $\ln(K_a)$  against  $T^{-1}$  graph (Figure 10), while  $\Delta G^0$  and  $\Delta S^0$  are obtained using Eq. 14 and Eq. 15.

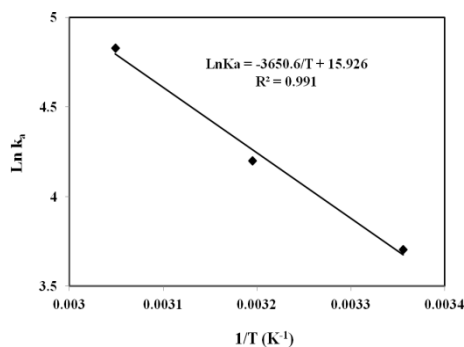


Fig. 10 Plot of  $\ln K_a$  versus the reciprocal temperature of arsenic ion adsorption by ZnOIn 3% nanopowder

Thermodynamic parameters are gathered in Table 6. Positive  $\Delta H^0$  indicates the endothermic character of the adsorption process. This is clearly evidenced by the enhancement of arsenic ions removal at elevated temperatures. Also the  $\Delta H^0$  value suggests an electrostatic attraction between As(III) ions and ZnOIn in a physical adsorption process. Moreover the positive value of  $\Delta H^0$  may be attributed to the eviction of hydration water molecules from the metal ions as well as solid–solution interface [46]. Thus the energy released when the ions are attached to the adsorbent surface will be used up by this dehydration process resulting in an endothermic sorption process [47] confirming the temperature study results. Moreover an increase in chaos at the interface between the solid and solution is revealed by the positive  $\Delta S^0$  values.

Table 6 Thermodynamic parameters for As(III) adsorption

Temperature (K)	K	$\Delta G^0$ (kJmol <sup>-1</sup> )	$\Delta S^0$ (kJmol <sup>-1</sup> K <sup>-1</sup> )	$\Delta H^0$ (kJmol <sup>-1</sup> )	$r^2$
298	1.1578	-9.637	0.1327		
313	1.3469	-11.649	0.1319	30.355	0.991
328	1.5934	-13.663	0.1327		

The data shown in Table 6, shows that  $\Delta G^0$  is negative with further decrease in its values as the temperature is increased. This designates the spontaneous character of the adsorption process, as well as its being favorable at elevated temperature.

#### 4. Comparative study

To ability of IZO nanopowder to eliminate As(III) is contrasted with that of other adsorption materials reported in literatures as recorded in Table 7. The juxtaposition between the findings obtained in this study with other adsorbents, manifests that IZO is highly effective in arsenic removal from aqueous solutions.

Table 7: A Comparison of IZO adsorption capacity with some nano-adsorbents for As(III)

Adsorbent	$q_e$ (mg·g <sup>-1</sup> )	Temp. (K)	pH	Ref.
Fe(III)-Si Binary Oxide	21.54	298	7	[7]
Activated carbon	-	298	7	[9]
Hazelnut shell	0.714	314	4-9	[11]
Char carbon	89	298	2-3	[48]
Activated carbon	29.9	298	6.4-7.5	[48]
TiO <sub>2</sub>	59.93	298	7	[49]
TiO <sub>2</sub> (Hombikat UV 1000)	22.7	295	4	[50]
MnO <sub>2</sub> -leaded resin	53	295	7-8.5	[51]
Zr resin	79.42	298	8	[52]
IZO	104	298	3	Present work
-	125	313	3	-
-	142	328	3	-
-	84	298	7	-

#### 5. Conclusions

This work described the elimination of As(III) ions from aqueous solutions using IZO nanopowder prepared by modified sol–gel method. The effects the initial arsenite concentration,

pH, temperature and indium-doping ratio were evaluated through batch-mode experiments. Results showed that the removal efficiency of As(III) was strongly pH dependent and optimum at pH 3 and 7. The adsorption equilibrium was found to comply with the Langmuir adsorption isotherm, with an utmost adsorption capacity of about 104.17 and 83.34 mgg<sup>-1</sup>, at pH 3 and 7, respectively. IZO nanopowder was effective for the As(III) removal, and data were found to comply with the pseudo-second-order kinetic model. The process of arsenite ions adsorption was an spontaneous endothermic physisorption.

### Acknowledgements

This work was supported by the National Plan, for Sciences, Technology and innovation, at Al-Imam Mohammed Ibn Saud Islamic University, college of Sciences, Kingdom of Saudi Arabia.

### References

- [1] F.W. Pontius, K.G. Brown, C.J. Chen, Am. Water Works Assoc. **86**, 52 (1994).
- [2] M.R.Karagas, T.A.Shukel, J.S. Morris, T.D.Tosteson, J.E. Weiss, S.K. Spencer, E.R.Greenberg, Am. J. Epidemiol. **153**, 559 (2001).
- [3] M.R.Karagas, T.D.Tosteson, J.Blum, Environ. Health Perspect. **106**, 1047 (1998).
- [4] Y. M.Kuo, C. W. Liu, K. H.Lin, Water Res. **38**, 148 (2004).
- [5] H.Takanashi, A. Tanaka, T. Nakajima, A.Ohki, Water Science and Technology **50**(8), 23 (2004).
- [6] I.N. Bhattacharya, P.K.Gochhayat, S. Paul, P.K.Mitra, The European Journal of Mineral Processing and Environmental Protection **5**(1), 1303 (2005), pp. 48 (2005).
- [7] L.Zeng, Water Qual. Res. J. Canada, **39**(3), 267 (2004).
- [8] B. P. Kelly, M. A.Tarek, Journal of Environmental Science and Health, **40**,723 (2005).
- [9] W.Yunhai, M.Xuhong, F. Maowu, L. Minmin, Journal of Hazardous Materials **159**, 380(2008).
- [10] A. M. Bruce, S. Goldberg. Clays and Cloy Minerals, **44**(5), 609 (1996).
- [11] D. N.Pravin, A. M. Kadam, H. S. Shankar, Journal of environmental biology, **30**(4), 499 (2009).
- [12] J. Benny, P. K. Manoj, V. K.Vaidyan, Bulletin of Materials Science, **28**(5), 487 (2005).
- [13] S.Girjesh, S. B.Shrivastava, J.Deepti, S.Pandya, T. Shripathi, V.Ganesan, Bulletin of Materials Science **33**(5), 581 (2010).
- [14] M. R.Rezaee, M.Behdani, H. Arabshahi, N.Hosseini, International Review of PHYSICS, **12**(3), 103 (2009).
- [15] Y.W. Chen, Y. C. Liu, S. X Lu, C.S.Xu, C. L. Shao, C Wang, J.Y. Zhang, Y.M. Lu, D. Z. Shen, X.W.Fan, J Chem Phys., **123**(13), 134701-(1-5) (2005).
- [16] L. El Mir, I. El Ghoul, S.Alaya, M. Ben Salem, Barthou C. abd Von Bardeleben H. J. J. Physica B, **403**, 1770 (2008).
- [17] L. El Mir, Z. Ben Ayadi, M.Saadoun, H.J. Von Bardeleben, K. Djessas, A.Zeinert, Phys. Stat. Sol. (a), **204**, 3266(2007).
- [18] B.C. Lippens, J.H. De Boer, J. Catalysis, **4**, 319 (1965).
- [19] R.Biswal, A. Maldonado, J. Vega-Pérez, D. R. Acosta, M.De La Luz Olvera, Starting from Zinc Acetylacetonate and Indium Chloride. Materials, **7**, 5038 (2014).
- [20] W. Tang, D.C.Cameron, Thin Solid Films. **238**(1), 83 (1994).
- [21] M.Hjiri, R.Dhahri, K.Omri, L.ElMir, S.G.Leonardi, N.Donato, G.Neri, Materials Sciencein Semiconductor Processing **27**,319 (2014).
- [22] Z. Ben Ayadi, L.ElMir, K. Djessas, S.Alaya, Thin Solid Films, **517**, 6305 (2009).
- [23] F.Rouquerol, J.Rouquerol, K.Sing, Adsorption by Powder and Porous Solids: Principles, Methodology and Applications, Academic Press. 1999.
- [24] N. Al Dahoudi, A.AlKahlout, S.Heusing, P.Herbeck-Engel, R. Karos, P.Oliveira,

- J. Sol-Gel SciTechnol, **67**, 556 (2013).
- [25] A.Alkahlout, N. Al Dahoudi, I.Grobelsek, M. Jilavi, P. W.de Oliveira, Journal of Materials, 2014, Article ID 235638, 8 pages. 2014.
- [26] X.Wang, W. Wang, X. Wang, J. Zhang, Z.Gu, L. Zhou, J. Ahao, RSC Adv. **5**, 4138 (2015).
- [27] S. Garcia, S.Sardar, S. Maldonado, V. Garcia, C.Tamez, J.G. Parsons, Microchemical Journal **117**, 52 (2014).
- [28] C.P. Huang, E.H.Smith, Chemistry in water reuse, Ann Arbor Science Publishers, Ann Arbor, Michigan, 2. 1981.
- [29] M. Jang, S.H. Min, T.H. Kim, J.K.Park Environ. Sci. Technol. **40**, 1636 (2006).
- [30] T. M.Thi, N. T. H. Trang, N. T. V.Anh, Applied Surface Science **340**, 166 (2015).
- [31] D.Morillo, G. Pérez, M. M.Valiente, Journal of Colloid and Interface Science **453**, 132 (2015).
- [32] V.K. Gupta, S. Sharma, I.S. Yadau, M.Dinesh, Journal Chemical Technology and Bio-thechnol. **71**, 180 (1889).
- [33] Y.S. Ho, G. Mckay, Chemical Engineering Journal, **70**, 115(1998).
- [34] K.J. Reddy, K.J. McDonald, H.King, Journal of Colloid and Interface Science **397**, 96 (2013).
- [35] S. Kong, Y. Wang, Q. Hu, A. K.Olusegun, Colloids and Surfaces A: Physicochemical and Engineering Aspect, **457**, 220 (2014).
- [36] W. J. Jr. Weber, J. C.Morris, J. Sanitary Eng. Div. Proceed. Am. Soc. Civil Eng. **89**, 31 (1963).
- [37] G.McKay,J. Chem. Technol. Biotechnol. A **33**, 196 (1983).
- [38] G. McKay, M.S. Otterburn, A.G.Sweeney, Water Res. **14**, 15 (1980).
- [39] M.Arami, N. Y Limaee, N. M. Mahmoodi, Chem. Eng. J. **139**(10), 2 (2008).
- [40] M.M.Benjamin, Effects of competing metals and complexing ligands on trace metal adsorption at the oxide/solution interface, PhD Thesis, Stanford University 1878.
- [41] B.E. Reed, M.R.Matsumoto, Separation Science and Technology, **28**(13 & 14), 97 (1993).
- [42] F. Hagheshresht, G.Lu, Energy Fuels **12**, 1100 (1998).
- [43] V.B.H. Dang, H.D. Doan, V. T. Dang, A.Lohi,Biores. Technol. **100**, 211 (2009).
- [44] MHorsfall, A. I. Spiff, A.A.Abia, Korean Chemical Society, 25(7), 969 2004.
- [45] J. Monika, V Garg, K.Kadirvelu, J. Hazardous materials **162**, 365 (2009).
- [46] M. Ricci, P. Spijker, K. Voitchovsky, Water-induced correlation between single ions imaged at the solid–liquid interface. Nat. Commun. **5**, 4400 doi: 10.1038/ncomms5400 (2014).
- [47] E.Tipping, Interactions of organic acids with inorganic and organic surfaces, in: E.M. Perdue, E.T. Gjessing (Eds.), Organic Acids in Aquatic Ecosystems. Life Sciences Research Reports, Wiley, New York, 209–221. 1990.
- [48] J.Pattanayak, K.Mondal, S. Mathew, S.B.Lalvani, Carbon **38**, 589 (2000).
- [49] M.E. Pena, G.P.Korfiatis, M. Patel, L. Lippincott, X.Meng, Water Res. **11**, 2327 (2005).
- [50] P.K.Dutta, A.K. Ray, V.K. Sharma, F.J.Millero, J. Colloid Interf. Sci.**278**, 270 (2004).
- [51] V.Lenoble, C.Chabroulet, R. Al Shukry, B.Serpaud, D. Véronique, J. C.Bollinger J. Colloid Interf. Sci.**280** (1), 62 (2004).
- [52] T.M. Suzuki, J.O.Bomani, H. Matsunaga, T.Yokoyama, React. Funct. Polym., **43**(1–2),165 (2000).